IEEE Photonics Journal
An IEEE Photonics Society Publication

Open Access

Compact Unidirectional Laser Based on All-Dielectric Metasurface With High Quality Factor

Volume 13, Number 1, February 2021

Ke Xu
Ming Fang, ***Member, IEEE***
Zhixiang Huang, ***Senior Member, IEEE***

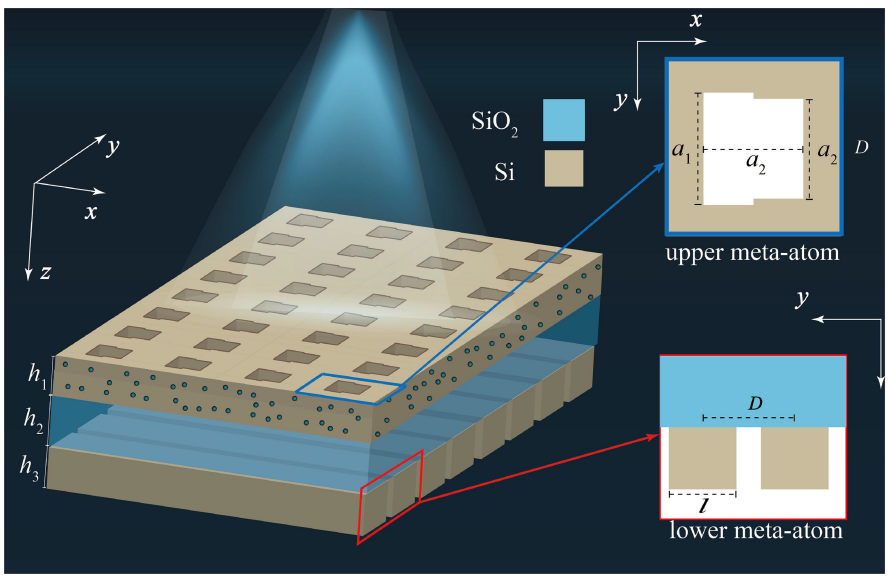

DOI: 10.1109/JPHOT.2020.3042818

Compact Unidirectional Laser Based on All-Dielectric Metasurface With High Quality Factor

Ke Xu, Ming Fang, *Member, IEEE*, and Zhixiang Huang, *Senior Member, IEEE*

Key Laboratory of Intelligent Computing and Signal Processing, Ministry of Education, and Key Laboratory of Electromagnetic Environmental Sensing, Department of Education of Anhui Province, Anhui University, Hefei 230601, China

DOI:10.1109/JPHOT.2020.3042818

Manuscript received September 8, 2020; revised November 27, 2020; accepted December 2, 2020. Date of publication December 7, 2020; date of current version December 31, 2020. This work was supported in part by the National Natural Science Foundation of China under Grants 61901001 and 61971001, in part by the National Natural Science Fund for Excellent Young Scholars under Grant 161722101, in part by the Natural Science Research Foundation of Anhui Province under Grant 1908085QF259, in part by the Natural Science Research Project of Anhui Universities under Grant 1KJ2019A0038, and in part by the Postdoctoral Researchers Foundation of Anhui Province under Grant 2019B347. Corresponding author: Ming Fang (e-mail: mingfang@ahu.edu.cn).

Abstract: All-dielectric metasurfaces offer unconventional optical functional behaviors for manipulating light, due to the strong localization of light with negligible dissipative loss. Here, we propose a compact design for a light emission cavity consist of an all-dielectric grating reflector and an all-dielectric symmetry-breaking metasurface supporting "dark" mode. The "dark" mode of the asymmetric metasurface structure results in high quality factor, and the broadband perfect reflector leads to directional emission. We present a theoretical study of the spectral characterization of the emission cavity, and the emission property of the nanocavity embedded with gain medium is investigated by a Maxwell-Bloch Langevin approach. Strong luminescence enhancement with directive light emission and reduced lasing threshold are observed. Our observations offer enormous potential in controlling light emission and provides an essential step for developing efficiency and directionality LEDs, and ultra-compact lasers.

Index Terms: Metasurfaces, dark mode, lasers, Maxwell-Bloch Langevin.

1. Introduction

Controlling light emission by enhanced light-matter interactions in nanostructures has been intensively investigated in regimes of sensing [1]–[3], quantum information devices [4], [5], efficiency enhanced solar cell [6]–[9], and lasers [10]–[12] owing to the strong localization of electromagnetic fields and long interaction times. Meanwhile, miniaturized nanoemitters and nanolasers are an emerging platform for manipulating light for quantum photonics. The conception of plasmonic nanostructures such as plasmonic metamaterials and plasmonic nanoantennas offers great flexibility for controlling light fields on a deep-subwavelength scale [13]–[16]. Endowed with the properties of plasmonic nanostructures, significant progresses have been made to control the laser characters and photoluminescence (PL) spectra of gain materials, such as plasmonic nanowire can lead to large enhancement of spontaneous emission, multifold enhancement and modification of the PL of

quantum dots (QDs) can be dominated by the plasmonic metamaterials [17]–[20]. However, relatively low Q-factors of these nanocavities owing to the intrinsic Joule losses at optical frequencies hamper the performance of metal-based nanoemitters.

Alternatively, using all-dielectric nanostructures is a promising way to overcome the dissipative losses in plasmonic ones. Recently, by coupling the gain medium with the collective resonance of all-dielectric metamaterials or by placing the gain medium in the nanogap of all-dielectric nanoparticles, emission intensity enhancement and significantly low lasing threshold have been experimentally achieved [21]–[25]. All-dielectric systems can provide high Q-factor modes with negligible loss, on the minus side, their size cannot go subwavelength due to the relatively low refractive index in the optical frequency range, and the strong radiation loss due to the "bright" mode also needs to overcome. To resolve these predicaments, nanocavities based on slightly symmetry-breaking "dark" modes or the interference between a "dark" state and a "bright" mode was proposed to reduce the radiative loss and to control the directionality of light emission on the subwavelength scale [26–34].

Here we propose a compact all-dielectric metasurface nanoemitter system. In our design, a silicon fishnet metasurface provides a high Q-factor nanocavity environment by introducing proper symmetry breaking and a silicon grating acts as a perfect reflector [35], [36] leading to unidirectional emission of the emitter. We first present the structure design and numerical simulation of the spectra characterization to reveal the principle of operation. Next, we exploit the lasing behaviors and luminescence characteristics of the nanoemitter with gain medium embedded in the nanocavity. In terms of numerical value, we propose a time-implementation of the Maxwell-Bloch Langevin approach [37]–[39] to model the semi-classical emission dynamics in quantum emitters (such as semiconductor quantum dots, quantum wells, and organic dyes) embedded in an arbitrary all-dielectric nanoemitters. Strong emission intensity enhancement and significantly reduced lasing threshold are observed which accompanied by a sharp Fano-type resonance.

2. Simulation Details

The proposed nanoemitter in our study is designed based on a silicon metasurface layer and a silicon grating layer. A schematic of the proposed nanoemitter is shown in Fig. 1(a). A glass interlayer is sandwiched between two silicon layers. The upper fishnet metasurface film with carved holes doped with gain medium provides coherent light emission. The film consists of a periodic lattice of asymmetric holes. The asymmetric hole is composed of symmetry breaking square as shown in Fig. 1(b). The lower layer is made up of a silicon grating having properly chosen height and periodicity to act as a broadband perfect reflector. Fig. 1(c) shows the cross-section of the grating mirror, the width of the silicon bar is properly optimized to $l = 400$ nm. The glass slab with a thickness of $h_2 = 200$ nm is sandwiched between the two silicon slabs to separate the silicon slabs. Silicon and glass are chosen because of their extremely low losses in the NIR/visible spectral range. Because of the polarization selection of grating reflectors, only when the incident electric field is along the *y*-direction, the grating has obvious wideband reflection characteristics. Therefore, by destroying the symmetry in the *y*-direction, the residual moment causes a *y*-polarized emission. In our design, the *y*-polarized emission is coupled to the metasurface structure, and the displacement current is induced inside the metasurface. The movement of these displacement currents can be equivalent to the oscillation of an electromagnetic dipole as shown in Fig. 2(e). A pair of antiphase dipoles is excited in each resonance element of the metasurface, the radiation components of two adjacent dipoles are offset by a destructive interference, resulting in a significant reduction in radiation loss, which appears as a "dark" mode. Since the dark mode is non-radiative, in order to make use of it, it is necessary to break the symmetry of the resonance element and make the resonance intensity of the two adjacent dipoles different. As illustrated in Fig. 2(f) most of the dipole radiation cancels with each other, and the residual dipole components (red arrow) form a discrete trapped mode resonance within the metasurface. The discrete trapped mode and the grating mode ("bright" mode) interference eventually form a Fano resonance. Ideally, as these structural units are periodic, the coupling of electromagnetic dipole oscillations in adjacent units

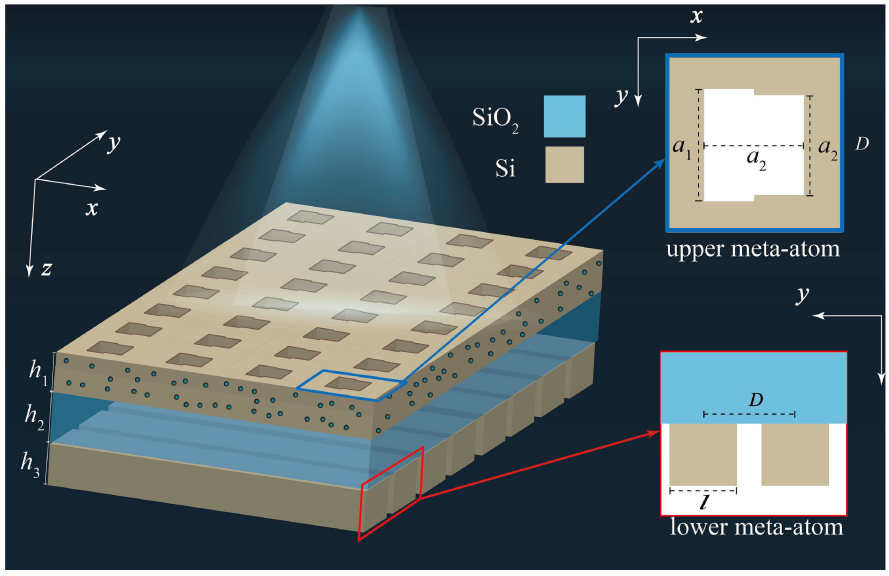

Fig. 1. (a) Schematic of the designed laser cavity. (b) The geometry of on unit cell of the dielectric fishnet metasurface. (c) Design of the grating reflector.

eventually forces all units in the plane to oscillate synchronously. This collective resonance behavior further improves the quality factor of the model, thus realizing the enhancement of luminescence in the nanostructure. Considering a more realistic case, the synchronous of the oscillations and the directionality are limited by the finite size of the metaruface and the pump source [34].

To determine the dimensions of the proposed nanoemitter and to explore the properties of the resonance modes, we employ the FDTD method [40]–[42] to simulate the spectra of the metasurface and grating under normal excitation by a transverse electric (*y*-polarized) wave. For the grating reflector with periodicity $D = 600$ nm, the electric dipole mode can be excited and can achieve ∼100% around the resonant peak as shown in Fig. 2(a). The structure can be tuned to achieve perfect reflection at different wavelengths with broad bandwidth by varying height of the silicon bar h_3. Based on the reflectance data shown in Fig. 2(a), we select $h_3 = 395$ nm. Fig. 2(b) shows the reflectance and transmittance as a function of wavelength, it shows that the reflectance over R $>$ 0.99 in the wavelength range from 1200 nm to 1450 nm. Fig. 2(c) shows the dispersion relation of the metasurface of thickness $h_1 = 400$ nm. Here, we choose the magnetic dipole mode, which has an antisymmetric electric field distribution and is therefore referring to the “dark” mode. The silicon fishnet metasurface not only overcomes the material losses but also reduces the radiation loss by the array effect. Ideally, the radiation loss can be totally suppressed if the periodic array is boundless, meanwhile, the spectral shape “dark” mode in the metasurface cannot exchange energy into external fields. Herein, we introduce a slightly antisymmetric nanohole in the fishnet for energy output coupling. Fig. 2(d) shows the spectrum of fishnet metasurface with symmetric holes (dashed curves) and asymmetric nanohole (solid curves). Due to the symmetry-breaking of the carved hole, sharp resonant spectra can be found around 1350 nm. In general, the interaction of the “bright” electric dipole of the grating layer and “dark” magnetic dipole of the metasurface exhibits monochromatic spectrum radiation with unidirectional scattering. Apparently, as the asymmetric nanoholes of fishnet metasurface tend to symmetric, weaker radiation damping leads to higher *Q* factor and lower lasing threshold. As a consequence, more laser energy at the operating frequency can be generated. However, there is a tradeoff between the radiation damping channel and the output coupling efficiency. While the radiation loss gets weaker and weaker, the *Q* factor increase and much more energy inside the metasurface will be simultaneously generated for the same pump

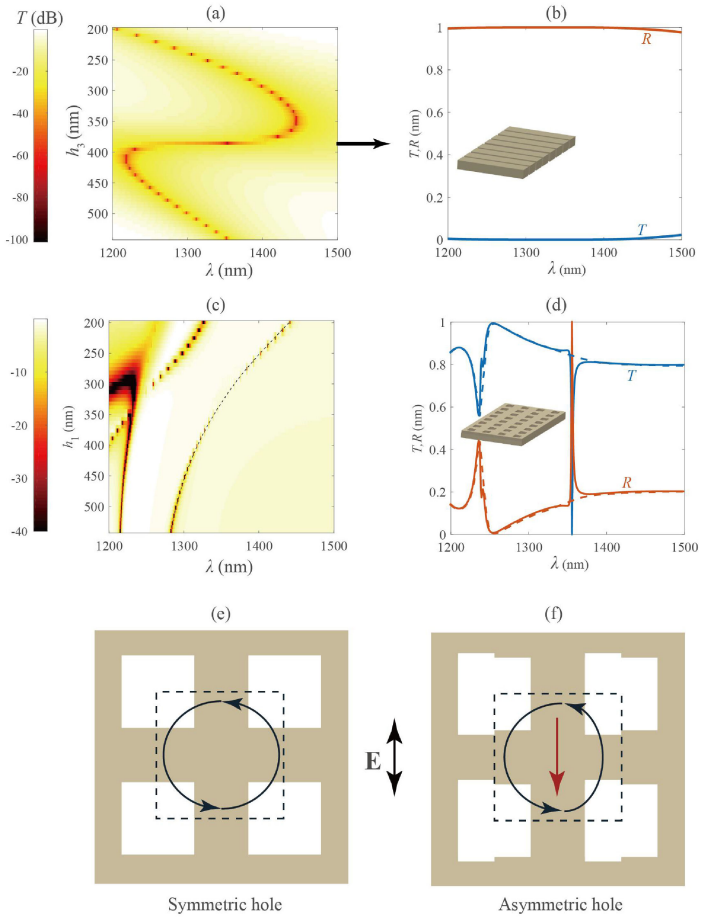

Fig. 2. Optimizations of the upper and lower reflectors. (a), (c) Transmission spectra of dark-state metasurface and grating with varied thickness. (b)The transmission and reflection spectra of optimized silicon grating ($h_3 = 395$ nm) for a broadband perfect reflector. (d) Spectra of metasurface at fixed values of $h_1 = 400$ nm, $a_1 = 400$ nm, the dashed lines indicate the spectra of metasurface with symmetric holes and the solid lines represent the spectra of metasurface with asymmetric holes. (e), (f) Illustrations of the destructive interferences of antiphase dipole in the metasurfaces with symmetric hole (e) and asymmetric hole (f), only the metasurface with asymmetric hole has residual dipole component remain (red arrow) and thus can exchange energy into external field.

power, but after some critical point, the output coupling efficiency will reduce and dominates the laser output. Thus, we need a rigorous physical model to investigate the interaction between gain medium and cavity mode self-consistently.

We investigate the gain medium embedded in the dielectric host material. To optimize the lasing cavity and explore the complex dynamical processes of gain materials in the metasurface based cavity, we apply a systematic theoretical model – a Maxwell-Bloch Langevin extended from the Maxwell-Bloch theory. Our starting point is the Maxwell equation for the classical electrodynamics

$$\begin{aligned} \nabla \times \mathbf{E} &= -\partial \mathbf{B}/\partial t \\ \nabla \times \mathbf{H} &= \varepsilon \varepsilon_0 \partial \mathbf{E}/\partial t + \partial \mathbf{P}/\partial t, \end{aligned} \tag{1}$$

where $\mathbf{P}$ is the electric polarization density. In general, the polarization can be expressed as $\mathbf{P} = \chi \varepsilon_0 \mathbf{E}$, and χ is the electric susceptibility. Note that $\mathbf{P}$ can be used to connect the Maxwell equations with multiphysics problems such as plasma fluid equations. Here, we model the Lorentz response of gain material by a four-level atomic system. The four-level system has two dipole

transitions for the absorption process (1↔2) and the emission process (0↔3), two non-radiative transfer processes with short lifetimes (3→2) and (1→0) are added to couple the two dipole transitions. The electron density on each level is $N_i (i = 0, 1, 2, 3)$. The time-dependent dispersive electric polarization density $\mathbf{P}$ corresponding to the transition dipole moment between level 2 and level 1 is driven by the external light and the population inversion $\Delta N = N_2 - N_1$, and its time evolution follows the Lorentzian oscillator

$$\begin{aligned}\frac{\partial^2 \mathbf{P}}{\partial t^2} = & -2\Gamma_e \frac{\partial \mathbf{P}}{\partial t} - \omega^2 \mathbf{P} - \sigma \left(N_2 - N_1\right) \mathbf{E} \\ & - \kappa \left(\omega \mathrm{Im}\left(F_{12}\right) + \frac{\partial \mathrm{Re}\left(F_{12}\right)}{\partial t}\right),\end{aligned} \tag{2}$$

here, the macroscopical polarization $\mathbf{P}$ and carrier densities N_i. σ are the phenomenological coupling constant of the local electric field to $\mathbf{P}$. The complex noise term F_{12} is associated with the polarization density. A simplified homogeneous pump mechanism is used, the external optical pump field is numerically simplified by a homogeneous pumping rate P_r. The pumping rate is equivalent to a pump intensity $I_p = \hbar\omega_e P_r N_e d$ [43] and $N_e = N_3 + N_2 + N_1 + N_0$ is total ion density in the gain medium. Thus, the polarization density of the absorption transition is neglected. The temporal evolution of the occupation numbers at each spatial point vary following the rate equations

$$\begin{aligned}\frac{\partial N_3}{\partial t} &= P_r N_0 - \frac{N_3}{\tau_{32}} - \frac{N_3}{\tau_{30}} + N_s F_{33} \\ \frac{\partial N_2}{\partial t} &= \frac{1}{\hbar\omega_e}\left(\frac{\partial \mathbf{P}_e}{\partial t} + \Gamma_e \mathbf{P}_e\right) \cdot \boldsymbol{\epsilon} + \frac{N_3}{\tau_{32}} - \frac{N_2}{\tau_{21}} + N_s F_{22} \\ \frac{\partial N_1}{\partial t} &= -\frac{1}{\hbar\omega_e}\left(\frac{\partial \mathbf{P}_e}{\partial t} + \Gamma_e \mathbf{P}_e\right) \cdot \boldsymbol{\epsilon} + \frac{N_2}{\tau_{21}} - \frac{N_1}{\tau_{10}} + N_s F_{11} \\ \frac{\partial N_0}{\partial t} &= -P_r N_0 + \frac{N_1}{\tau_{10}} + \frac{N_3}{\tau_{30}} + N_s F_{00},\end{aligned} \tag{3}$$

here the polarization densities $\mathbf{P_e}$ of the transition $1 \leftrightarrow 2$, Γ_e is the emission linewidth, N_s is the number of atoms in a grid cell. The noise terms $\hat{F}_{ii} (i = 0, 1, 2, 3)$ related to the population densities and polarization can be derived by the fluctuation-dissipation theorem [44]

$$\left\langle \hat{F}_i(t) \hat{F}_j(t) \right\rangle = \left(\frac{d}{dt}\left\langle \hat{A}_i \hat{A}_j \right\rangle\right)_{NH} - \left\langle \hat{D}_i \hat{A}_j \right\rangle - \left\langle \hat{A}_i \hat{D}_j \right\rangle, \tag{4}$$

The subscript "NH" after the bracket denotes that only dissipative terms (non-Hamiltonian) terms are to be included. $\hat{A}$ and $\hat{D}$ are the dynamic operator and dissipation operator. Thus, the stochastic noise terms related to the pumping and dissipation of the atomic density matrix. Therefor the stochastic noise terms related to the pumping and dissipation of the atomic density matrix can be calculated from Eq. (3). Then the noise terms in the emission polarization density equation and rate equations can be derived as

$$\begin{aligned}F_{12} &= \left(\mathrm{Re}\left(\xi_{12}\right) + i\mathrm{Im}\left(\xi_{12}\right)\right) \sqrt{\left\langle \hat{F}_{12} \hat{F}_{12}^* \right\rangle N_s} \\ &= \left(\mathrm{Re}\left(\xi_{12}\right) + i\mathrm{Im}\left(\xi_{12}\right)\right) \sqrt{\gamma_{32} N_3 + \left(2\Gamma_e - \gamma_{21}\right) N_2} \\ F_{00} &= \xi_{10} \sqrt{\left\langle \hat{F}_{12} \hat{F}_{12}^* \right\rangle N_s} = \xi_{10} \sqrt{\gamma_{10} N_1} \\ F_{11} &= -\xi_{10} \sqrt{\gamma_{10} N_1} \\ F_{22} &= \xi_{32} \sqrt{\gamma_{32} N_3} \\ F_{33} &= -\xi_{32} \sqrt{\gamma_{32} N_3},\end{aligned} \tag{5}$$

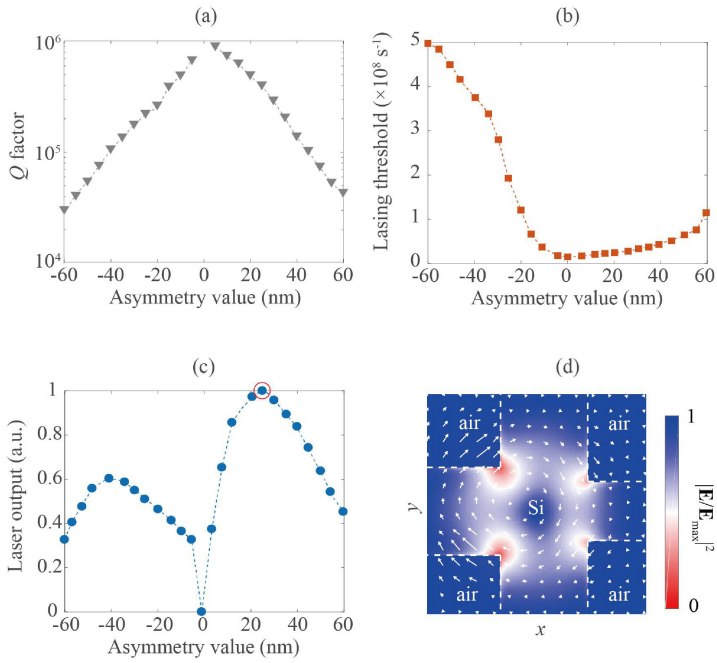

Fig. 3. Numerical simulation results for optimized $h_1 = 400$ nm and $h_3 = 395$ nm. Asymmetric value dependence of (a) Q factor, (b) lasing threshold, and (c) lasing amplitude. (d) The electric field profile and field vector distribution on the fishnet metasurface (x-y plane) during lasing.

here ξ_{ij} are random, Gaussian variables with zero mean fulfilling the two-time correlation and can be generated by the ziggurate algorithm [45]. The set of multiphysics equations (1) – (3) and (5) can be self-consistently solved with the help of a parallel 3D auxiliary differential equation finite-different time-domain (ADE-FDTD) code. This method enables us not only to simulate on the nanoscale spatiotemporal evolution of light fields in arbitrary geometry plasmonic and all-dielectric environment but also includes coherent fields and spontaneous emissions in gain media. With the help of the proposed method, we investigate how the all-dielectric laser cavity affects the emission properties of a gain medium. In the simulation, the gain medium is embedded in the fishnet metasurface of permittivity $\varepsilon_r = 12.1$. The parameters of gain medium are sets as: a density of $N = 5 \times 10^{23}\,\mathrm{m}^{-3}$, lifetimes $\tau_{10} = \tau_{32} = 50$fs and $\tau_{21} = 50$ps, emission frequency $\omega_e = 2\pi \times 215 \times 10^{12}\,\mathrm{rad/s}$, emission linewidth $\Gamma_e = 10\tau\eta z$, and coupling strength $\sigma = 1 \times 10^{-4}\mathrm{C}^2/\mathrm{kg}$. For a given pumping rate P_r, the electron density in each level is saturated before lasing and can be given by solving Eq. (3)

$$\begin{aligned} N_3 &= N_e\tau_{32}P_r/((\tau_{10}+\tau_{21}+\tau_{32})P_r+1) \\ N_2 &= N_e\tau_{21}P_r/((\tau_{10}+\tau_{21}+\tau_{32})P_r+1) \\ N_1 &= N_e\tau_{10}P_r/((\tau_{10}+\tau_{21}+\tau_{32})P_r+1) \\ N_0 &= N_e/((\tau_{10}+\tau_{21}+\tau_{32})P_r+1), \end{aligned} \tag{6}$$

Thus, the lengthy pump process in the simulation can be skipped by using the initial electron densities in Eq. (6).

Fig. 3(a) and (b) show evolutions of the Q factor and the lasing threshold when the asymmetric of the hole changes. For "dark" mode induced by the symmetry breaking, the asymmetric value $a_1 - a_2$ determines the Q factor and threshold pump power as expected, namely, the Q factor of "dark" mode decreases monotonously as the asymmetric size $a_1 - a_2$ gets larger. The laser output in Fig. 3(c) and Q factor present different variations tendency. As the asymmetric size becomes smaller and smaller, the laser output increase, but after some point ($|a_1 - a_2| = 25$nm)

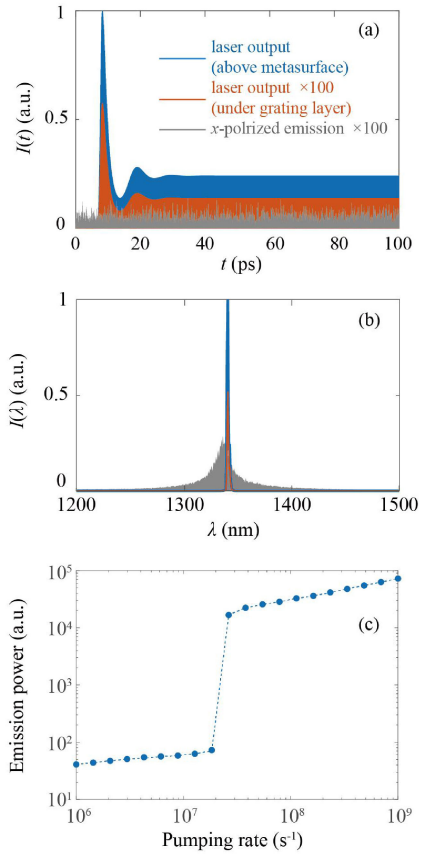

Fig. 4. Dynamics of the intensity of (a) *y*-polarized emission calculated above the metasurface (blue curve) and under the grating layer (red curve), *x*-polarized emission (gray curve). The intensity of the red curve and the gray curve is scaled up by a factor of 100. The *x*-polarized emission trace shows typical spontaneous emission (noise) dynamics, indicating that the laser cavity is of specific polarization properties (b) Intensity spectra corresponding to the time traces in (a). (c) The emission power as a function of pumping rate.

the laser output will not further increase and diverge. The lasing amplitude reaches the highest point at asymmetric value $a_1 - a_2 = 20$nm. It is worth noting that in the case of symmetric holes ($a_1 - a_2 = 0$nm), the laser output almost vanishes. This is because the net dipole moment of the "dark" mode is totally canceled and the output coupling efficiency is zero. The field distribution of a symmetry-breaking case plotted during the lasing in Fig. 3(d) exhibits that the two nearby electric oscillations in the *x*-direction are out-of-phase but have the same amplitude. This leads to the complete cancellation of the coherent laser field in the *x*-direction, and only the *y*-polarized laser output can be observed in the far-field.

The laser cavity studied here shows prominent polarization characteristic and distinct directionality. Fig. 4 shows the emission dynamics and spectra of the optimized configuration $a_1 - a_2 = +25$nm(marked as red circle in Fig. 3(c)). The pumping rate used in this simulation is lower than the laser threshold without the metasurface. It is noticed that the grating layer provides broadband perfect reflection leading to directional emission. Fig. 4(a) shows the dynamics of *y*-polarized emission recorded above the metasurface and under the grating layer. It is worth noting that the laser field almost only emitted from the surface of the fishnet metasurface. The other notable thing is the asymmetric of the fishnet metasurface leads to a specific distribution of the "dark" mode and finally controls the polarization property of the laser cavity. Without the high *Q*-factor mode in the *x*-direction, only noisy spontaneous emission is observed in the *x*-polarized field as plotted by the

gray lines. The spectra corresponding to Fig. 4(a) are shown in Fig. 4(b) by Fourier transforming the time-domain fields. Fig. 4(c) shows the emission power as a function of pumping rate at wavelength ~1350 nm. The laser threshold is clearly observed while pumping rate reaches $P_r = 2.6 \times 10^7 s^{-1}$.

3. Conclusion

In summary, we demonstrated a compact nanolaser with high-directionality based on all-dielectric metasurface. We observed that low lasing threshold and strong lasing enhancement achieved using the subwavelength nanoemitters. It should be noted that the design of the metasurface cavity is free from Ohmic loss and more compact compared to plasmonic designs and the Bragg cavity. Our observations and the proposed method offer a deep insight into the mechanism of the complex interactions between nanocavities and quantum emitters, paving the way for the design of efficient LEDs, lasers, and displays based on active metasurfaces. In addition, the Maxwell-Bloch Langevin theory was shoved with the help of the FDTD algorithm for modeling and capturing the quantum behaviors and strong optical nonlinearities in the gain materials. The proposed concepts may pave the way toward densely packed quantum nanoemitters and the nanocavities with tunable power nanoscale lasing sources. Our designs offer prospects to realize high-directionality, high-efficiency, low lasing threshold LEDs, displays and functional lasers.

References

[1] S. Lal, S. Link, and N. J. Halas, "Nano-optics from sensing to waveguiding," *Nat. Photon.*, vol. 1, no. 11, pp. 641–648, 2007.
[2] A. V. Kabashin *et al.*, "Plasmonic nanorod metamaterials for biosensing," *Nat. Mater.*, vol. 8, no. 11, pp. 867–871, 2009.
[3] L. Polavarapu and L. M. Liz-Marzán, "Towards low-cost flexible substrates for nanoplasmonic sensing," *Physical Chemistry Chem. Phys.*, vol. 15, no. 15, pp. 5288–5300, 2013.
[4] R. W. Heeres, L. P. Kouwenhoven, and V. Zwiller, "Quantum interference in plasmonic circuits," *Nat. Nanotechnol.*, vol. 8, no. 10, pp. 719–722, 2013.
[5] M. S. Tame, K. R. McEnery, Ş. K. Özdemir, J. Lee, S. A. Maier, and M. S. Kim, "Quantum plasmonics," *Nat. Phys.*, vol. 9, no. 6, pp. 329–340, 2013.
[6] S. Pillai, K. R. Catchpole, T. Trupke, and M. A. Green, "Surface plasmon enhanced silicon solar cells," *J. Appl. Phys.*, vol. 101, no. 9, pp. 093105-1–093105-8, 2007.
[7] K. Nakayama, K. Tanabe, and H. A. Atwater, "Plasmonic nanoparticle enhanced light absorption in gaas solar cells," *Appl. Phys. Lett.*, vol. 93, no. 12, 2008, Art. no. 121904.
[8] V. E. Ferry *et al.*, "Light trapping in ultrathin plasmonic solar cells," *Opt. Exp.*, vol. 18, no. S2, pp. A237–A245, 2010.
[9] H. A. Atwater and A. Polman, "Plasmonics for improved photovoltaic devices," *Nat. Mater.*, vol. 9, no. 3, pp. 205–213, 2010.
[10] H. G. Park *et al.*, "Electrically driven single-cell photonic crystal laser," *Science*, vol. 305, no. 5689, pp. 1444–1447, 2004.
[11] O. Hess, J. B. Pendry, S. A. Maier, R. F. Oulton, J. M. Hamm, and K. L. Tsakmakidis, "Active nanoplasmonic metamaterials," *Nat. Mater.*, vol. 11, no. 7, pp. 573–584, 2012.
[12] N. Shankhwar *et al.*, "High-quality laser cavity based on all-dielectric metasurfaces," *Photon. Nanostructures - Fundamentals Appl.*, vol. 24, pp. 18–23, 2017, doi: 10.1016/j.photonics.2017.02.003.
[13] C. M. Soukoulis, S. Linden, and M. Wegener, "PHYSICS: Negative refractive index at optical wavelengths," *Science*, vol. 315, no. 5808, pp. 47–49, 2007.
[14] J. Henzie, M. H. Lee, and T. W. Odom, "Multiscale patterning of plasmonic metamaterials," *Nat. Nanotechnol.*, vol. 2, no. 9, pp. 549–554, 2007.
[15] A. Babynina, M. Fedoruk, P. Kühler, A. Meledin, M. Döblinger, and T. Lohmüller, "Bending gold nanorods with light," *Nano Lett.*, vol. 16, no. 10, pp. 6485–6490, 2016.
[16] S. Arena, F. Cucinotta, O. Di Stefano, A. Cacciola, R. Saija, and S. Savasta, "Plasmonic absorption enhancement of a single quantum dot," *Plasmonics*, vol. 10, no. 4, pp. 955–962, 2015.
[17] R. F. Oulton *et al.*, "Plasmon lasers at deep subwavelength scale," *Nature*, vol. 461, no. 7264, pp. 629–632, 2009.
[18] K. Tanaka, E. Plum, J. Y. Ou, T. Uchino, and N. I. Zheludev, "Multifold enhancement of quantum dot luminescence in plasmonic metamaterials," *Phys. Rev. Lett.*, vol. 105, no. 22, pp. 227403-1–227403-4, 2010.
[19] P. Viste *et al.*, "Enhancement and quenching regimes in metal–semiconductor hybrid optical nanosources," *ACS Nano*, vol. 4, no. 2, pp. 759–764, 2010.
[20] H. R. Hamedi and M. R. Mehmannavaz, "Behavior of optical bistability in multifold quantum dot molecules," *Laser Phys.*, vol. 25, no. 2, 2015, Art. no. 025403.
[21] N. Shankhwar, R. K. Sinha, Y. Kalra, S. Makarov, A. Krasnok, and P. Belov, "High-quality laser cavity based on all-dielectric metasurfaces," *Photon. Nanostructures - Fundam. Appl.*, vol. 24, pp. 18–23, 2017.
[22] S. Romano *et al.*, "Surface-Enhanced raman and fluorescence spectroscopy with an all-dielectric metasurface," *J. Phys. Chem. C*, 2018, doi: 10.1021/acs.jpcc.8b03190.

[23] S. T. Ha *et al.*, "Directional lasing in resonant semiconductor nanoantenna arrays," *Nat. Nanotechnol.*, to be published, doi: 10.1038/s41565-018-0245-5.
[24] A. Vaskin *et al.*, "Directional and spectral shaping of light emission with mie-resonant silicon nanoantenna arrays," *ACS Photon.*, vol. 5, no. 4, pp. 1359–1364, 2018.
[25] V. Yannopapas and I. E. Psarobas, "Lasing action in multilayers of alternating monolayers of metallic nanoparticles and dielectric slabs with gain," *J. Opt.*, vol. 14, no. 3, 2012, Art. no. 035101.
[26] J. Zhang, K. F. MacDonald, and N. I. Zheludev, "Near-infrared trapped mode magnetic resonance in an all-dielectric metamaterial," *Opt. Exp.*, vol. 21, no. 22, 2013, Art. no. 26721.
[27] J. Zhang, W. Liu, Z. Zhu, X. Yuan, and S. Qin, "Strong field enhancement and light-matter interactions with all-dielectric metamaterials based on split bar resonators," *Opt. Exp.*, vol. 22, no. 25, 2014, Art. no. 30889.
[28] C. Zhou, S. Li, Y. Wang, and M. Zhan, "Multiple toroidal dipole fano resonances of asymmetric dielectric nanohole arrays," *Phys. Rev. B*, vol. 100, no. 19, pp. 195306-1–195306-8, 2019.
[29] C. Cui *et al.*, "Multiple fano resonances in symmetry-breaking silicon metasurface for manipulating light emission," *ACS Photon.*, to be published, doi: 10.1021/acsphotonics.8b00754.
[30] S. Yuan *et al.*, "Strong photoluminescence enhancement in all-dielectric fano metasurface with high quality factor," *ACS Nano*, vol. 11, no. 11, pp. 10704–10711, 2017.
[31] S. Droulias, A. Jain, T. Koschny, and C. M. Soukoulis, "Novel lasers based on resonant dark states," *Phys. Rev. Lett.*, vol. 118, 2017, Art. no. 073901.
[32] S. Droulias, A. Jain, T. Koschny, and C. M. Soukoulis, "Fundamentals of lasers based on resonant dark states," *Phys. Rev. B*, vol. 96, 2017, Art. no. 155143.
[33] T. K. Hakala *et al.*, "Lasing in dark and bright modes of a finite-sized plasmonic lattice," *Nat. Commun.*, vol. 8, 2017, Art. no. 13687.
[34] S. Droulias, T. Koschny, and C. M. Soukoulis, "Finite-size effects in metasurface lasers based on resonant dark states," *ACS Photon.*, vol. 5, no. 9, 2018, Art. no. 3788.
[35] S. Kim *et al.*, "Monolithic high-contrast grating based polariton laser," *ACS Photon.*, vol. 6, no. 1, pp. 18–22, 2019.
[36] C. J. ChangHasnain, "High-contrast gratings as a new platform for integrated optoelectronics," *Semicond. Sci. Technol.*, vol. 26, no. 26, 2010, Art. no. 014043.
[37] J. Andreasen and H. Cao, "Creation of new lasing modes with spatially nonuniform gain," *Opt. Lett.*, vol. 34, no. 22, 2009, Art. no. 3586.
[38] S. Wuestner *et al.*, "Gain and plasmon dynamics in active negative-index metamaterials," *Phys. Eng. Sci.*, vol. 369, no. 1950, pp. 3525–3550, 2011.
[39] A. Pusch, S. Wuestner, J. M. Hamm, K. L. Tsakmakidis, and O. Hess, "Coherent amplification and noise in gain-enhanced nanoplasmonic metamaterials: A maxwell-bloch langevin approach," *ACS Nano*, vol. 6, no. 3, pp. 2420–2431, 2012.
[40] A. Taflove and S. C. Hagness, "Computational Electrodynamics: The Finite-difference Time-domain Method," 3rd ed., Norwood, MA, USA: Artech House, 2005.
[41] M. Fang, Z. Huang, T. Koschny, and C. M. Soukoulis, "Electrodynamic modeling of quantum dot luminescence in plasmonic metamaterials," *ACS Photon.*, vol. 3, no. 4, pp. 558–563, 2016.
[42] Z. Huang, T. Koschny, and C. M. Soukoulis, "Theory of pump-probe experiments of metallic metamaterials coupled to a gain medium," *Phys. Rev. Lett.*, vol. 108, 2012, Art. no. 187402.
[43] *For a Thin Gain Slab Illuminated By a Plane Wave the Pumping Rate is Equivalent to the Pump Intensity. The pump Power Density is Equal to* $\hbar\omega$*ePrN0, and the Pump Intensity Ipump = (Pump Power)/(Surface Area) =* $\hbar\omega$*ePrN0 (volume)/(surface area) =* $\hbar\omega$*ePrN0d*; here d is the thickness of the gain slab.
[44] A. Pusch, S. Wuestner, and J. M. Hamm, "Coherent amplification and noise in gain-enhanced nanoplasmonic metamaterials: A maxwell-bloch langevin approach," *ACS Nano*, vol. 6, no. 3, 2012, Art. no. 2420.
[45] G. Marsaglia and W. W. Tsang, "The ziggurat method for generating random variables," *J. Statal Softw.*, vol. 5, no. 8, 2000, doi: 10.18637/jss.v005.i08.